Int. J. Heat Mass Transfer. Vol. 36, No. 5, pp. 1159–1170, 1993
Printed in Great Britain

0017–9310/93 $6.00 + 0.00

The effect of perfectly conducting side walls on natural convection in porous media

PETER VADASZ
Department of Mechanical Engineering, University of Durban-Westville, Private Bag X54001, Durban 4000, South Africa

and

CAROL BRAESTER and JACOB BEAR
Faculty of Civil Engineering, Technion–Israel Institute of Technology, Haifa 32000, Israel

(*Received* 20 *November* 1991 *and in final form* 10 *June* 1992)

Abstract—An investigation of natural convection in a porous medium heated from below or above, and bounded by perfectly conducting side walls, shows that a motionless solution is impossible, except for a particular side wall temperature variation. Hence, convection occurs regardless of the value of Rayleigh number and regardless of whether the fluid is heated from below or from above. Numerical solutions for identical uniform temperatures imposed on both side walls (no temperature difference between the side walls) show that when heating from below, a subcritical flow results mainly near the side walls, which amplifies and extends over the entire domain under supercritical conditions.

1. INTRODUCTION

THE SCOPE of this study is to analyze the effect of perfectly conducting side walls on natural convection in porous media. General conclusions are drawn from the analysis of the governing equations and numerical solutions are presented for a two-dimensional rectangular porous domain, of which results are compared to analytical solutions obtained for imperfectly insulated side walls, showing good qualitative agreement.

Natural convection in porous media is of considerable interest in geophysics and engineering. Heat transfer in geothermal systems (see Cheng [1, 2] for a comprehensive review) and the insulation technology may serve as examples for the occurrence of this phenomenon. Natural convection in porous media has been studied in the past under the following conditions: (a) heating from the side, (b) heating from below (or above), and (c) the combined heating from the side and above.

Different temperatures imposed on the side walls (case (a)) were studied by Bejan and Tien [3]. It was shown that such conditions lead to a unicellular fluid motion. With an increase in the Rayleigh number, the intensity of the flow amplifies and different flow and heat transfer regimes can be identified. Heating from below (case (b)) is generally treated as a stability problem. This problem was investigated for different top and bottom boundary conditions (see refs. [4–9]). It was found that fluid motion is possible only if the Rayleigh number exceeds a critical value. Theoretical and experimental investigations show that supercritical Rayleigh number values lead to multicellular fluid motion. No motion is expected when the fluid is heated from above, regardless of the Rayleigh number. In such cases the vertical temperature gradient resulting from heating the upper boundary and/or cooling the lower boundary is considered to be a stabilizing temperature gradient. The effect of a weak heat leakage through imperfectly insulated side walls on natural convection in a rectangular porous domain heated from below was investigated analytically by Vadasz and Braester [10]. The analytical solution obtained through the weak non-linear theory showed that a small heat leakage through the side walls directly affected the solution at the leading order and the preferred wave number of convection. A comparison study regarding multiple solutions and the corresponding bifurcations resulting from analytical solutions to this problem was presented by Vadasz [11].

The combined effect of heating from the side and above (case (c)), a case of practical interest in thermal insulation design, was studied by Kimura and Bejan [12]. It was expected that the convection driven by differentially heating from the sides could be suppressed by imposing a stabilizing vertical temperature gradient. Numerical solution showed that convection can be suppressed only partly. Kimura and Bejan concluded that "... the side driven natural convection does not disappear completely even when the vertical stabilizing gradient is greater than the destabilizing horizontal gradient". Similar conclusions were

NOMENCLATURE

$\hat{\mathbf{e}}_x$	unit vector in the x direction
$\hat{\mathbf{e}}_y$	unit vector in the y direction
$\hat{\mathbf{e}}_z$	unit vector in the z direction
$\hat{\mathbf{e}}_g$	unit vector in the direction of the gravity acceleration
$\mathbf{g}_*$	gravity acceleration vector
H_*	height of the domain
k_*	permeability
L_*	length of the domain
L	aspect ratio, defined as $L = L_*/H_*$
M_f	a ratio between the heat capacity of the fluid and the effective heat capacity of the domain
p	pressure
p_a	pressure related to a hydrostatic and adiabatic reference value
$\mathbf{q}$	Darcy's volumetric flux
Ra	Rayleigh number
r	a numerical parameter, defined as $r = \Delta t/\Delta L^2$
s	a numerical parameter, defined as $s = \Delta t/2\Delta L$
$\mathbf{S}$	a vector, defined in the text following equation (6)
t	time
T	temperature
u	Darcy's volumetric flux component in the x direction
w	Darcy's volumetric flux component in the z direction
$\mathbf{X}$	position vector, equal to $x\hat{\mathbf{e}}_x + y\hat{\mathbf{e}}_y + z\hat{\mathbf{e}}_z$.

Greek symbols

α_{e*}	effective thermal diffusivity of the porous medium
β_*	thermal expansion coefficient
ε	an expansion parameter, defined in the text following equation (18)
θ	side walls heat flux, defined by equation (18)
μ_*	dynamic viscosity
ν_*	kinematic viscosity
ρ_*	density
ψ	stream function, defined in the text preceding equation (16)
ω	vorticity vector, defined in the text preceding equation (6).

Subscripts

*	dimensional quantity
0	reference value
b	related to the bottom
c	characteristic value
e	effective value
H	related to the horizontal
t	related to the top
w	related to the side walls.

achieved experimentally by Ostrach and Raghavan [13] for fluid in a non-porous domain.

If this conclusion is generally true, then by lowering the horizontal temperature difference on the lateral boundaries the flow should not stabilize completely. The limit of such a process would be a zero horizontal temperature difference, i.e. equal temperatures imposed on the lateral walls. This is recognized to be the case of heating from below (or above) with perfectly conducting lateral boundaries. Practically, this situation is obtained particularly in thin lateral walls made of materials which have high thermal conductivity. This is the subject of the present investigation. Through the analysis of the governing equations we show that except for a particular linear temperature variation on the lateral boundaries, it is impossible to obtain a fluid motionless state under perfectly conducting lateral boundary conditions. A numerical solution of the governing equations is presented for identical uniform temperatures imposed on both lateral boundaries. Its results compare favorably with the qualitative analytical solution obtained for the case of imperfectly insulated side walls.

2. THE GOVERNING EQUATIONS AND PROBLEM FORMULATION

We consider an isotropic and homogeneous porous matrix with respect to permeability and to thermal conductivity. Except for fluid density, which is considered to be temperature dependent, all other properties, e.g. permeability and thermal conductivity, are assumed to be constant. The temperature difference between the solid matrix and the fluid, within a representative elementary volume, around a point is assumed to be negligible [14]. The dispersion of heat is considered small in comparison to the advective and conductive terms in the energy equation [15]. We also assume Oberbeck–Boussinesq's approximation [16, 17]. Under these conditions the governing equations are:

(i) Equation of continuity

$$\nabla \cdot \mathbf{q} = 0 \tag{1}$$

(ii) Momentum balance equation (Darcy's law)

$$\mathbf{q} = -[\nabla p_a + RaT\nabla(\hat{\mathbf{e}}_g \cdot \mathbf{X})] \tag{2}$$

(iii) Energy balance equation

$$\frac{\partial T}{\partial t} + \mathbf{q} \cdot \nabla T = \nabla^2 T \tag{3}$$

where the dimensionless variables are defined as

$$\mathbf{X} = \mathbf{X}_*/H_*, \quad t = t_* \alpha_{c*}/H_*^2 M_f, \quad \mathbf{q} = \mathbf{q}_* H_* M_f/\alpha_{c*},$$
$$p_a = p_{a*} k_* M_f/\mu_* \alpha_{c*}, \quad T = (T_* - T_0)/\Delta T_c,$$
$$\hat{\mathbf{e}}_g = \mathbf{g}_*/|\mathbf{g}_*| \tag{4}$$

and the Rayleigh number is defined in the form

$$Ra = \frac{\beta_* \Delta T_c g_* k_* H_*}{\alpha_{c*} \nu_*} M_f. \tag{5}$$

In equations (4) and (5), $\mathbf{q}_*$ is Darcy's flux, t_* is time, $\mathbf{X}_*$ denotes the position vector, H_* is a characteristic length of the flow domain (e.g. the height, when a rectangular domain is considered), k_* is the permeability, μ_* is the dynamic viscosity of the fluid, T_0 and ΔT_c are a reference temperature and a characteristic temperature difference, respectively, $\mathbf{g}_*$ is the gravity acceleration vector and p_a is the pressure related to an adiabatic hydrostatic reference value. In the definition of the Rayleigh number, equation (5), ν_* is the kinematic viscosity of the fluid, α_{c*} is the effective thermal diffusivity, M_f is the heat capacity ratio, g_* is the absolute value of the gravity acceleration and β_* is the thermal expansion coefficient. We concentrate the discussion on generally closed domains, D, bounded by impermeable boundaries, B. These kinds of boundaries imply the boundary condition $\mathbf{q}_n \cdot \hat{\mathbf{e}}_n|_B = 0$.

A condition for the existence of a motionless solution

For the subsequent analysis it is convenient to define the vorticity vector ω as $\omega = \nabla \times \mathbf{q}$, and by applying the curl operator $(\nabla \times\ )$ to equation (2) one obtains the vorticity equation

$$\omega = -Ra\mathbf{S} \tag{6}$$

where the vector $\mathbf{S}$ is defined as $\mathbf{S} = \nabla \times (T\hat{\mathbf{e}}_g)$. Equation (6) shows that the vorticity, ω, is obtained by multiplying the Rayleigh number by the vector $\mathbf{S}$. Since the vector $\mathbf{S}$ directly affects the vorticity, it is of interest to discuss its properties. In a Cartesian coordinate system with the z axis oriented upwards, the vectors $\hat{\mathbf{e}}_g$, $\mathbf{S}$ and the horizontal thermal gradient, $\nabla_H T$, are expressed as: $\hat{\mathbf{e}}_g = -\hat{\mathbf{e}}_z$; $\mathbf{S} = -(\partial T/\partial y)\hat{\mathbf{e}}_x + (\partial T/\partial x)\hat{\mathbf{e}}_y$; $\nabla_H T = (\partial T/\partial x)\hat{\mathbf{e}}_x + (\partial T/\partial y)\hat{\mathbf{e}}_y$, respectively, and the position vector $\mathbf{X}$ is defined as $\mathbf{X} = x\hat{\mathbf{e}}_x + y\hat{\mathbf{e}}_y + z\hat{\mathbf{e}}_z$, where $\hat{\mathbf{e}}_x$, $\hat{\mathbf{e}}_y$ and $\hat{\mathbf{e}}_z$ are the unit vectors in the x, y and z directions, respectively. The following properties of the vector $\mathbf{S}$ hold in any domain $D \in R^3$ and are direct consequences of the definitions of $\hat{\mathbf{e}}_g$, $\mathbf{S}$ and $\nabla_H T$:

(P1) The vectors $\mathbf{S}$ and $\nabla_H T$ are orthogonal, i.e. $\mathbf{S} \cdot \nabla_H T = 0 \ \forall \ \mathbf{X} \in D$.

(P2) The magnitudes of the vectors $\mathbf{S}$ and $\nabla_H T$ are equal, i.e. $\mathbf{S} \cdot \mathbf{S} = \nabla_H T \cdot \nabla_H T \ \forall \ \mathbf{X} \in D$.

(P3) Both vectors $\mathbf{S}$ and $\nabla_H T$ are orthogonal to the gravity acceleration vector, $\hat{\mathbf{e}}_g$, i.e. $\mathbf{S} \cdot \hat{\mathbf{e}}_g = 0$ and $\nabla_H T \cdot \hat{\mathbf{e}}_g = 0 \ \forall \ \mathbf{X} \in D$.

The following conclusions based on the properties (P1) and (P2) are important for the subsequent stages of this analysis.

$$\mathbf{S} = 0 \Leftrightarrow \nabla_H T = 0. \tag{7}$$

A sufficient condition for the occurrence of natural convection is therefore expressed in the form

$$\mathbf{S} \neq 0 \Rightarrow \mathbf{q} \neq 0. \tag{8}$$

Now by using (7) one obtains

$$\nabla_H T \neq 0 \Rightarrow \mathbf{q} \neq 0. \tag{9}$$

The main conclusion resulting from (9) is that the necessary condition for the existence of a motionless state is: $\nabla_H T = 0 \ \forall \ \mathbf{X} \in D$. As a result, whenever horizontal thermal gradients exist, natural convection currents are produced. An example of cases when natural convection exists unconditionally are vertical layers or rectangular domains subject to different values of temperature at the side walls. As a result of this horizontal temperature difference the heat will be transferred initially mainly by conduction, thus creating horizontal thermal gradients in the fluid-saturated porous domain, i.e. $\nabla_H T \neq 0$. These horizontal thermal gradients create unconditional convection based on the previous analysis. A horizontal infinite layer or a rectangular porous domain heated from below are examples of cases when the equations and the appropriate boundary conditions can be satisfied by motionless conduction solutions, leading to vanishing of any horizontal thermal gradients in the domain. In these cases the motionless conduction solutions represent the equilibrium or basic solutions, whose stability should be investigated. Obviously, due to the non-linear nature of the thermal convection effect, represented by the non-linear coupled differential equations, non-uniqueness of the possible solutions may result and the stability analysis may contribute to determine which solution is expected to occur.

For horizontal infinite layers or rectangular porous domains with *perfectly insulated side walls* heated from below, the linear stability analysis shows that fluid motion is possible only if the Rayleigh number exceeds a critical value. Theoretical and experimental investigations show that supercritical Rayleigh number values lead to multicellular fluid motion. The linear stability analysis does not usually predict the amplitude and direction of the convective flow. No motion is expected when the fluid is heated from above, regardless of the value of the Rayleigh number. In such cases the vertical temperature gradient resulting from heating the upper boundary and/or cooling the lower boundary is considered to be a stabilizing temperature gradient.

However, for *perfectly conducting side walls* differ-

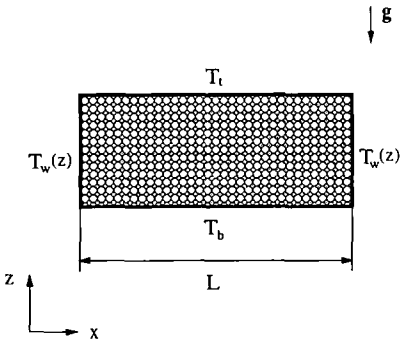

FIG. 1. A two-dimensional porous domain with perfectly conducting side walls.

ent conclusions can be drawn. Let us consider a rectangular domain $D \in R^2$ (Fig. 1) and the following boundary conditions: $T = T_b$ at $z = 0$, $T = T_t$ at $z = 1$ and $T = T_w(z)$ at $x = 0$ and $x = L$. It can be observed that the same temperature is imposed on both side walls so there is *no horizontal temperature difference* between the side walls. One may distinguish between heating from below, i.e. $T_b = 1$ and $T_t = 0$, and heating from above, when $T_b = 0$ and $T_t = 1$. Then it will be shown that with perfectly conducting side walls, except for the linear distribution of temperature on the side walls, $T_w \neq (T_t - T_b)z + T_b$, natural convection occurs independently of the value of the Rayleigh number (obviously different from zero). To show this, the proof is given by negation for the extreme case of heating from above. The proof of heating from below is similar. Therefore, upon using $T_b = 0$ and $T_t = 1$ pertaining to heating from above, it will be proved that if

$$T_w(z) \neq z \tag{10}$$

then

$$\mathbf{q} \neq 0. \tag{11}$$

Let us assume that under condition (10) a motionless solution ($\mathbf{q} = 0$) is possible. Then the heat is transferred only by conduction and the steady state energy equation (3) reduces to

$$\nabla^2 T = 0. \tag{12}$$

However, the necessary condition for the existence of a motionless state resulting from equation (9) is expressed for a two-dimensional domain in the form

$$\frac{\partial T}{\partial x} = 0 \; \forall \; \mathbf{X} \in D. \tag{13}$$

Moreover, if (13) holds then also $\partial^2 T/\partial x^2 = 0 \; \forall \; \mathbf{X} \in D$. Substitution of these conditions into (12) yields

$$\frac{d^2 T}{dz^2} = 0 \tag{14}$$

of which solution is given by the linear profile

$$T = z. \tag{15}$$

This solution, which is consistent with a motionless state ($\mathbf{q} = 0$), satisfies the boundary conditions at $x = 0$, L if and only if (i) $T_w = z$ or (ii) $(\partial T/\partial x)_{x=0,L} = 0$. The first case, (i), is contradictory to the data as expressed by (10). The second case, (ii), does not correspond to perfectly conducting side walls. We may conclude that the results expressed by conditions (i) and (ii), found by assuming that a motionless state is possible, are contradictory to the basic assumptions. *Therefore, a motionless state is not possible in connection with the data considered.*

A prescribed constant temperature on the lateral boundaries, $T = T_w = \text{const.}$ (the same value at both lateral walls), is an example of a problem for which a motionless solution is not possible, regardless of the vertical temperature gradient resulting from the imposed top and bottom boundary conditions. Practically, this situation is obtained particularly in thin lateral walls made of materials which have high thermal conductivity. This specific case is considered in the following numerical solution. However, before presenting the numerical solution a comparison between this case and the analytical results obtained for the case of imperfectly insulated side walls is performed.

3. A WEAK HEAT FLUX THROUGH THE SIDE WALLS

For a constant prescribed temperature on the side walls (perfectly conducting side walls), a strong heat flux occurs on the lateral walls. However, with imperfectly insulated side walls the lateral heat flux is weak and an analytical solution is possible through the weak non-linear theory. The detailed analysis and solution for the imperfectly insulated side walls case was presented by Vadasz and Braester [10]. Only the minimum necessary results will be repeated here for the purpose of comparison with the perfectly conducting side walls case. The governing equations (1), (2) and (3) for a two-dimensional rectangular domain were expressed for convenience in terms of a stream function and temperature. A Cartesian coordinate system was selected such that the vertical axis, z, is collinear with the gravity axis and directed upwards; then $\hat{\mathbf{e}}_g = -\hat{\mathbf{e}}_z$ and in (2) $\hat{\mathbf{e}}_g \cdot \mathbf{X} = -z$. Applying the curl operator to equation (2) and using the definition of the stream function ψ: $u = \partial\psi/\partial z$, $w = -\partial\psi/\partial x$, where u and w are Darcy's flux components in the x and z directions, respectively, one obtains from (2) and (3)

$$\nabla^2 \psi + Ra \frac{\partial T}{\partial x} = 0 \tag{16}$$

$$\frac{\partial T}{\partial t} - \nabla^2 T + \frac{\partial \psi}{\partial z}\frac{\partial T}{\partial x} - \frac{\partial \psi}{\partial x}\frac{\partial T}{\partial z} = 0. \tag{17}$$

In terms of ψ, the flow boundary conditions are expressed in the form: $\psi = 0 \; \forall \; \mathbf{X} \in B$, and the thermal boundary conditions for heating from below are

$z=0$: $T=1$; $z=1$: $T=0$; $x=0$: $\partial T/\partial x=\theta_0(z)$, $x=L$: $\partial T/\partial x=\theta_L(z)$. The side walls heat flux is represented by a sine Fourier expansion in the form

$$\theta_0(z)=\sum_{k=1}^{r}\theta_{0k}\sin(k\pi z);\quad \theta_L(z)=\sum_{k=1}^{r}\theta_{Lk}\sin(k\pi z). \tag{18}$$

To be consistent with a basic motionless state, the side wall heat leakages θ_0 and θ_L are assumed to be small, i.e. $\theta_0(z)\ll 1$, $\theta_L(z)\ll 1\ \forall\ z\in[0,1]$. The dependent variables ψ and T were expanded in a power series in terms of a small parameter, ε, defined as $\varepsilon^2=(Ra-Ra_c)/Ra$, where Ra_c is the characteristic value of Ra obtained from the linear stability analysis, $Ra_c=\pi^2(m^2+n^2L^2)^2/m^2L^2$, where m and n are the wave numbers in the x and z directions, respectively, and L is the aspect ratio (length/height). The Fourier coefficients in (18) were also expanded in a power series of ε and the Rayleigh number was expanded in a finite power series. Therefore, the expansions are expressed in the form

$$\begin{aligned}[\psi,T,\theta_{0k},\theta_{Lk}]=&[\psi^{(0)},T^{(0)},\theta_{0k}^{(0)},\theta_{Lk}^{(0)}]\\&+\varepsilon[\psi^{(1)},T^{(1)},\theta_{0k}^{(1)},\theta_{Lk}^{(1)}]\\&+\varepsilon^2[\psi^{(2)},T^{(2)},\theta_{0k}^{(2)},\theta_{Lk}^{(2)}]\\&+\varepsilon^3[\psi^{(3)},T^{(3)},\theta_{0k}^{(3)},\theta_{Lk}^{(3)}]+O(\varepsilon^4)\end{aligned} \tag{19}$$

$$Ra=Ra_c+Ra_c^{(2s)}[\varepsilon^2+\varepsilon^4+\cdots+\varepsilon^{2s}] \tag{20}$$

where $\psi^{(0)}$ and $T^{(0)}$ represent the basic motionless solution, i.e. $\psi^{(0)}=0$ and $T^{(0)}=1-z$. In order to avoid an inconsistency and occurrence of resonance at orders ε and ε^2, $\theta_{0k}^{(1)}$, $\theta_{Lk}^{(1)}$, $\theta_{0k}^{(2)}$ and $\theta_{Lk}^{(2)}$ must vanish. Thus the heat leakage through the side walls was introduced at order ε^3, i.e. $\theta_{0k}^{(3)}\neq 0$ and $\theta_{Lk}^{(3)}\neq 0$, while $\theta_{0k}^{(1)}=\theta_{Lk}^{(1)}=\theta_{0k}^{(2)}=\theta_{Lk}^{(2)}=0$. Introduction of these expansions into equations (16) and (17) and collecting terms which include like powers of ε leads to a hierarchy of partial differential equations for the different orders. The solutions of the homogeneous equations at order ε subject to homogeneous boundary conditions lead to the following eigenfunctions:

$$\psi^{(1)}=A_{mn}^{(1)}(\tau)\sin(m\pi x/L)\sin(n\pi z);$$

$$T^{(1)}=B_{mn}^{(1)}(\tau)\cos(m\pi x/L)\sin(n\pi z)$$

where the amplitudes $A_{mn}^{(1)}$ and $B_{mn}^{(1)}$ are allowed to vary slowly over the large time scale $\tau=\varepsilon^2 t$ in order to overcome time non-uniformity of the solutions. At this stage the amplitudes are still undetermined and their values will be obtained later from a solvability condition of the equations at order ε^3.

The qualitative form of the solutions at order ε^2 is the same as for order ε except for an additional term, $B_{02n}^{(2)}\sin(2n\pi z)$, in the expression for $T^{(2)}$ which occurs as a result of the non-homogeneous type of equation for $T^{(2)}$. The equations at order ε^3 are

$$\nabla^2\psi^{(3)}+Ra_c\frac{\partial T^{(3)}}{\partial x}=-Ra_c^{(2)}\frac{\partial T^{(1)}}{\partial x} \tag{21}$$

$$\begin{aligned}\nabla^2T^{(3)}-\frac{\partial\psi^{(3)}}{\partial x}=&\frac{\partial T^{(1)}}{\partial\tau}+\frac{\partial\psi^{(1)}}{\partial z}\frac{\partial T^{(2)}}{\partial x}-\frac{\partial\psi^{(1)}}{\partial x}\frac{\partial T^{(2)}}{\partial z}\\&+\frac{\partial\psi^{(2)}}{\partial z}\frac{\partial T^{(1)}}{\partial x}-\frac{\partial\psi^{(2)}}{\partial x}\frac{\partial T^{(1)}}{\partial z}\end{aligned} \tag{22}$$

and their right-hand side represents their non-homogeneous part, which consists of known lower order solutions $\psi^{(1)}$, $T^{(1)}$, $\psi^{(2)}$ and $T^{(2)}$ and their derivatives. At this order the heat leakage through the side walls is introduced leading to the following boundary conditions:

$$x=0:\partial T^{(3)}/\partial x=\theta_0^{(3)}(z)=\sum_{k=1}^{r}\theta_{0k}^{(3)}\sin(k\pi z)$$

and

$$x=L:\partial T^{(3)}/\partial x=\theta_L^{(3)}(z)=\sum_{k=1}^{r}\theta_{Lk}^{(3)}\sin(k\pi z).$$

The remaining boundary conditions are homogeneous, i.e. $\psi^{(3)}(0,z)=\psi^{(3)}(L,z)=\psi^{(3)}(x,0)=\psi^{(3)}(x,1)=0$ and $T^{(3)}(x,0)=T^{(3)}(x,1)=0$. Since equations (21) and (22) at order ε^3 are non-homogeneous versions of the equations solved at order ε, a solvability condition must be satisfied. This condition constrains the amplitude of the solution at order ε and enables its determination. The solvability condition is derived by multiplying (21) by $\psi^{(1)}$ and (22) by $Ra_cT^{(1)}$, integrating these equations over the domain $x\in[0,L]$, $z\in[0,1]$ and adding them. As a result of these operations and by some mathematical manipulations, use of the second Green's identity, integration by parts, boundary conditions and the solutions at $O(\varepsilon)$, the solvability condition for the steady state may be presented in the simplified form

$$A^3-\xi A=\eta \tag{23}$$

where the following notation is used for convenience:

$$\chi=\frac{\pi^2}{8L^2};\quad A=-\varepsilon mA_{mn}^{(1)};$$

$$\xi=8(m^2+n^2L^2)[Ra/Ra_c-1];$$

$$\eta=-\frac{16(m^2+n^2L^2)}{\pi}[\theta_{0n}-(-1)^m\theta_{Ln}];$$

$$\theta_{0n}=\varepsilon^3\theta_{0n}^{(3)};\quad \theta_{Ln}=\varepsilon^3\theta_{Ln}^{(3)}. \tag{24}$$

In (24), A represents the $O(\varepsilon)$ amplitude, ξ is the measure of how distant Ra is from its critical value ($\xi=0$ at $Ra=Ra_c$, $\xi<0$ for $Ra<Ra_c$ and $\xi>0$ for $Ra>Ra_c$) and η represents the small $O(\varepsilon^3)$ heat leakage through the side walls. As one may observe from the expression of η in (24), in spite of the general expansion for the heat leakage through the side walls which was allowed to include all possible Fourier modes, only those modes which reinforce the natural modes of convection, i.e. $k=n$, affect the amplitude equation through η. In the following, the particular

case of symmetrical heat leakage through the side walls will be considered, i.e. $\theta_{0n} = -\theta_{Ln} = \theta_n$ and $\eta = -[32(m^2+n^2L^2)\theta_n]/\pi \; \forall \; m = 2, 4, 6, 8 \ldots$; $\eta = 0$ $\forall \; m = 1, 3, 5, 7 \ldots$ as this is associated with symmetrical heat fluxes occurring in the perfectly conducting case. For perfectly insulated side walls, $\eta = 0$, leading to the amplitude solution of equation (23) in the form $A = \pm\xi^{1/2}$ for $\xi > 0$ ($Ra > Ra_c$) and $A = 0$ for $\xi < 0$ ($Ra < Ra_c$). This solution is represented by the dotted curves in Fig. 2, showing a bifurcation of the amplitude solution towards two possible branches. As a result, the direction of the flow (clockwise or anticlockwise) for supercritical conditions is undetermined as the amplitude of the convection, A, can be positive or negative corresponding to the respective branch of the bifurcation ($A = +\xi^{1/2}$ or $A = -\xi^{1/2}$). For the imperfectly insulated case $\eta \neq 0$ and according to (23) the motionless state, $A = 0$, does not satisfy the equation. The solution of the non-homogeneous cubic equation (23) is represented by the full curves in Fig. 2. It can be observed that the sharp transition at the critical value of $Ra(\xi = 0)$ in the perfect case ($\eta = 0$) is replaced by a smooth transition through Ra_c ($\xi = 0$) in the imperfect case ($\eta \neq 0$). In the latter case (with imperfectly insulated side walls) a non-zero subcritical amplitude was obtained for $Ra < Ra_c$. For supercritical Ra values ($Ra > Ra_c$), a unique steady solution was obtained as long as $0 < \xi < 3(\eta/2)^{2/3}$. This unique solution is independent of the initial conditions associated with the corresponding time-dependent amplitude equation (see Vadasz and Braester [10]) and therefore in this range of ξ values, *the flow intensity and direction are absolutely controlled by the boundary imperfection through η. The higher the side walls heat flux the wider the domain for ξ where this conclusion applies.* An immediate implication resulting from this solution is that a convection cell rotates clockwise or anticlockwise depending on whether the heat flux at the side walls is directed outwards or inwards to the domain. For example, considering the first mode of the sine series representing the side walls heat flux with a positive value of θ_1, i.e. $(\partial T/\partial x)_{x=0} = \theta_1 \times \sin(\pi z)$ and $(\partial T/\partial x)_{x=L} = -\theta_1 \sin(\pi z)$ with $\theta_1 > 0$, a heat flux directed from the domain outwards is obtained on the side walls. As a result, according to the conclusions of the weak non-linear solution this heat flux should create an anticlockwise convection in the vicinity of the left side wall (at $x = 0$) and a clockwise convection near the right side wall (at $x = L$). When θ_1 is negative ($\theta_1 < 0$), the flow direction of the convection cells reverses, i.e. it is clockwise near the left side wall and anticlockwise near the right side wall. An important particular case is when the fundamental is absent in the sine series expansion of the side walls heat flux. Then the second mode of the sine series becomes dominant, i.e. $(\partial T/\partial x)_{x=0} = \theta_2 \sin(2\pi z)$, $(\partial T/\partial x)_{x=L} = -\theta_2 \sin(2\pi z)$ with $\theta_2 > 0$; this implies that the heat flux is directed outwards at the lower half of the domain, i.e. for $z \in [0, 1/2]$ and inwards at the upper half of the domain, i.e. for $z \in [1/2, 1]$. This type of heat flux induces, according to the weak non-linear analysis, the second vertical mode of convection consisting of two overlaying rows of convection cells, the lower rotating anticlockwise near the left wall and clockwise near the right wall and the upper rotating clockwise near the left wall and anticlockwise near the right wall. Assuming that these results will remain qualitatively unchanged even for strong heat fluxes through the side walls they can

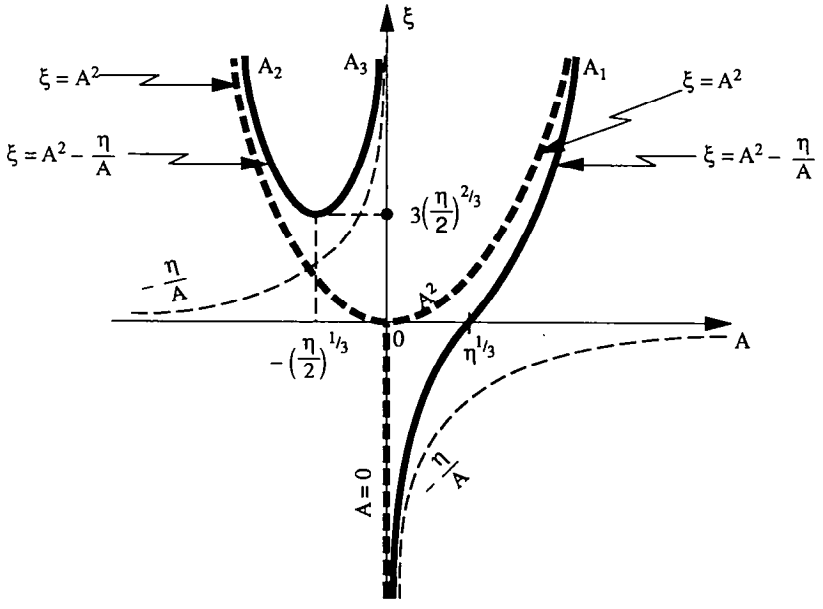

FIG. 2. Graphical representation of the amplitude solutions in the ξ–A plane.

be applied for confirmation of the numerical results obtained for the perfectly conducting case, to be presented in the next sections.

4. PERFECTLY CONDUCTING SIDE WALLS

A prescribed constant temperature on the side walls, $T = T_w = \text{const.}$ (*the same value at both side walls*), is an example of a problem with perfectly conducting side walls. For this case a strong heat flux occurs on the side walls, and a motionless solution is not possible regardless of the vertical temperature gradient resulting from the imposed top and bottom boundary conditions.

The problem to be solved numerically is formulated as a two-dimensional initial boundary value problem in terms of the stream function ψ and temperature T, according to equations (16) and (17). These equations form the coupled system to be solved numerically subject to the impermeability boundary condition $\psi = 0 \; \forall \; \mathbf{X} \in B$ and the thermal boundary conditions, which consist of two different cases:

heating from below:

$$T_b = 1, \quad T_t = 0$$

heating from above:

$$T_b = 0, \quad T_t = 1 \tag{25}$$

where T_b and T_t are the bottom and top temperatures, respectively. For each of the above cases three possible subcases, related to the temperature on the lateral boundaries, are considered

$$T_w < 0 \tag{26a}$$

$$1 < T_w \tag{26b}$$

$$0 < T_w < 1. \tag{26c}$$

These three subcases correspond to the different directions of the heat fluxes at the side walls, e.g. when the heating is from below, case (a) represents a heat flux oriented from the domain outwards, case (b) is compatible with an inward heat flux at the side walls and in case (c) the heat flux is outwards at the bottom half of the side walls ($z \in [0, 1/2]$) and inward at the top half of the side walls ($z \in [1/2, 1]$). For heating from above the directions of the heat fluxes at the side walls remain unchanged for cases (a) and (b) but are reversed for case (c).

The numerical method of solution consists of a fully implicit finite difference scheme for the energy equation, (17), and centered differences for the elliptic stream function, equation (16). A uniform spatial mesh is used throughout the rectangular domain, i.e. $\Delta x = \Delta z = \Delta L$. By using a single index notation to represent the mesh points, the following difference equation is obtained for the temperature:

$$a_{i,i-N} T_{i-N}^{j+1} + a_{i,i-1} T_{i-1}^{j+1} + a_{i,i} T_i^{j+1} + a_{i,i+1} T_{i+1}^{j+1} + a_{i,i+N} T_{i+N}^{j+1} = T_i^j \; \forall \; i = 1, 2, \ldots, M \times N \tag{27}$$

where $(M+1)$ and $(N+1)$ are the number of mesh points in the x and z directions, respectively. The indices $(j+1)$ and (j) denote the present and the preceding time, respectively. The coefficients of T^{j+1} are expressed by

$$a_{i,i-N} = -(su_i + r); \quad a_{i,i-1} = -(sw_i + r);$$

$$a_{i,i} = (1 + 4r); \quad a_{i,i+1} = (sw_i - r);$$

$$a_{i,i+N} = (su_i - r) \tag{28}$$

where $r = \Delta t / \Delta L^2$, $s = \Delta t / 2\Delta L$ and u_i, w_i are the mesh point values of the horizontal and vertical components of $\mathbf{q}$, respectively. The difference equation (27) represents a system of $(M \times N)$ linear equations for the $(M \times N)$ unknown values of temperature T_i^{j+1} $(i = 1, 2, \ldots, M \times N)$ at the mesh points. The components of the right-hand side vector consist of the known values of temperature at the preceding time step and additional terms which include the values of the temperature on the boundary. These additional terms should be transferred from the left-hand side of (27) whenever boundary mesh points appear. The coefficients, (28), form a five band matrix. However, they depend on the solution of the stream function equation through u_i and w_i. The difference equation for the stream function is obtained from (16) by using centered differences. Then, with the single index notation, it can be expressed in the form

$$\psi_{i-N}^{j+1} + \psi_{i-1}^{j+1} - 4\psi_i^{j+1} + \psi_{i+1}^{j+1} + \psi_{i+N}^{j+1} = Ra \frac{\Delta L}{2} [T_{i-N}^{j+1} - T_{i+N}^{j+1}] \; \forall \; i = 1, 2, \ldots, M \times N. \tag{29}$$

This equation represents a system of $(M \times N)$ linear equations for the unknown values of ψ_i^{j+1} at the mesh points $i = 1, 2, \ldots, M \times N$. The coefficients form a five band matrix and they are constants; however, the right-hand side of equation (29) depends on the unknown temperature values T_i^{j+1}. Therefore, the two systems of equations (27) and (29) are coupled. An iterative procedure is used at every time step to solve this coupling. Therefore, at every time step equation (27) is solved for T_i^{j+1} by using a band solver [19]. The values of u_i and w_i are initially identical to the previous time step values, i.e. u_i^j, w_i^j. Then the temperature values are introduced into (29) and a solution for ψ_i^{j+1} is obtained by using the same band solver. New values of u_i and w_i are calculated by introducing ψ_i^{j+1} into the centered difference form of the stream function's definition. This procedure is repeated with the new values of u_i and w_i until the maximum relative difference between two consecutive iterations is less than a prescribed tolerance ε_{it}, i.e.

$$\max_{i = 1, 2, \ldots, M \times N} [|\Delta \psi_i^{j+1}| / |\psi_i^{j+1}|] < \varepsilon_{it}$$

and

$$\max_{i = 1, 2, \ldots, M \times N} [|\Delta T_i^{j+1}| / |T_i^{j+1}|] < \varepsilon_{it}. \tag{30}$$

Then the solution is advanced by an additional time step until the steady state is achieved, according to the following criterion:

$$\max_{i=1,2,\ldots,M\times N}[|\psi_i^{j+1}-\psi_i^j|/|\psi_i^{j+1}|] < \delta \qquad (31)$$

where δ is the steady state prescribed tolerance.

5. RESULTS AND DISCUSSION

The results obtained by using the numerical method of solution described in Section 4 are presented for two different cases, i.e. heating from below ($T_b = 1$, $T_t = 0$) and heating from above ($T_b = 0$, $T_t = 1$). Three subcases related to each of the foregoing cases are considered according to (26). Therefore, three different values of the lateral wall temperature were imposed:

(i) $T_w = -0.5$, (ii) $T_w = 1.5$, (iii) $T_w = 0.5$

such that cases (i), (ii) and (iii) correspond to (26a), (26b) and (26c), respectively.

All the cases were solved for an aspect ratio of 1 : 2 ($L = 2$), and the following grid and tolerance parameters: $\Delta L = 0.05$ (41×21), $\Delta t = 0.001$ and $\varepsilon_{ij} = 0.001$. Finer grids were occasionally used for evaluation of accuracy and numerical error analysis. All the runs started from motionless initial conditions and from uniform initial temperature, which was set equal to the value of T_w corresponding to each specific case.

5.1. *Heating from below*

Several runs have been performed for different values of the Rayleigh number. Subcritical convection was obtained when $Ra = 30$ ($Ra_c = 4\pi^2$), as a result of the lateral boundary heat flux. A supercritical steady state solution is presented in Fig. 3 for $Ra = 50$ and $T_w = -0.5$, corresponding to subcase (i) and to (26a). The isotherms and streamlines show that the solution consists of two convection cells. The direction of rotation of the left cell is anticlockwise as predicted analytically through the weak non-linear solution.

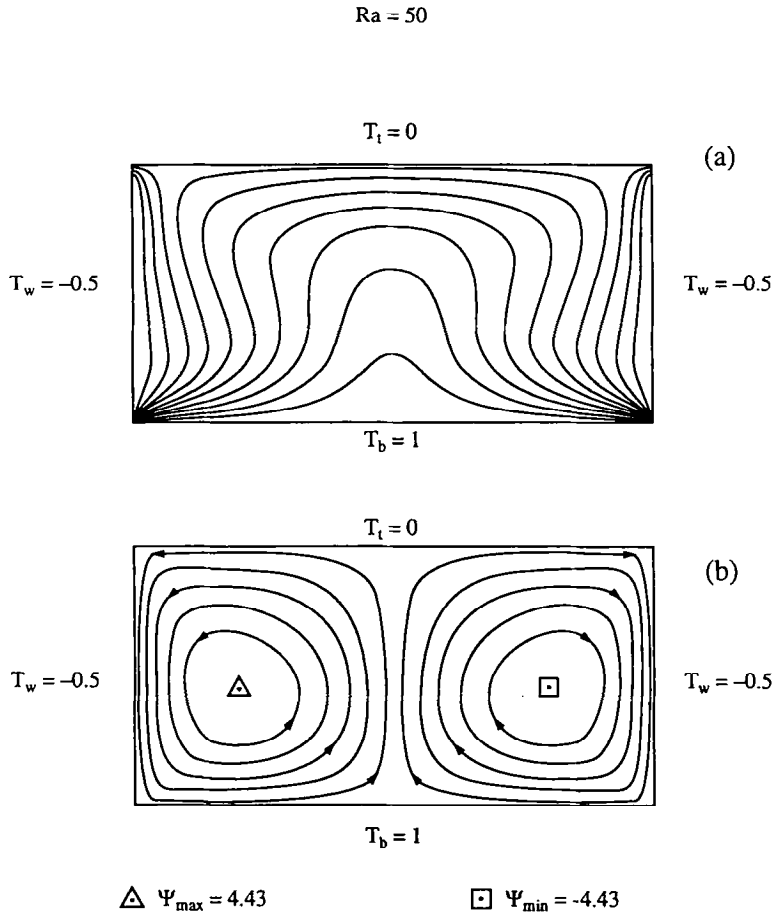

FIG. 3. Graphical representation of the numerical solutions for the flow and temperature fields for heating from below, corresponding to $Ra = 50$ and $T_w = -0.5$. (a) Ten isotherms equally divided between T_{min} and T_{max} ($T_{min} = -0.5$, $T_{max} = 1$). (b) Ten streamlines equally divided between ψ_{min} and ψ_{max} ($\psi_{min} = -4.43$, $\psi_{max} = 4.43$).

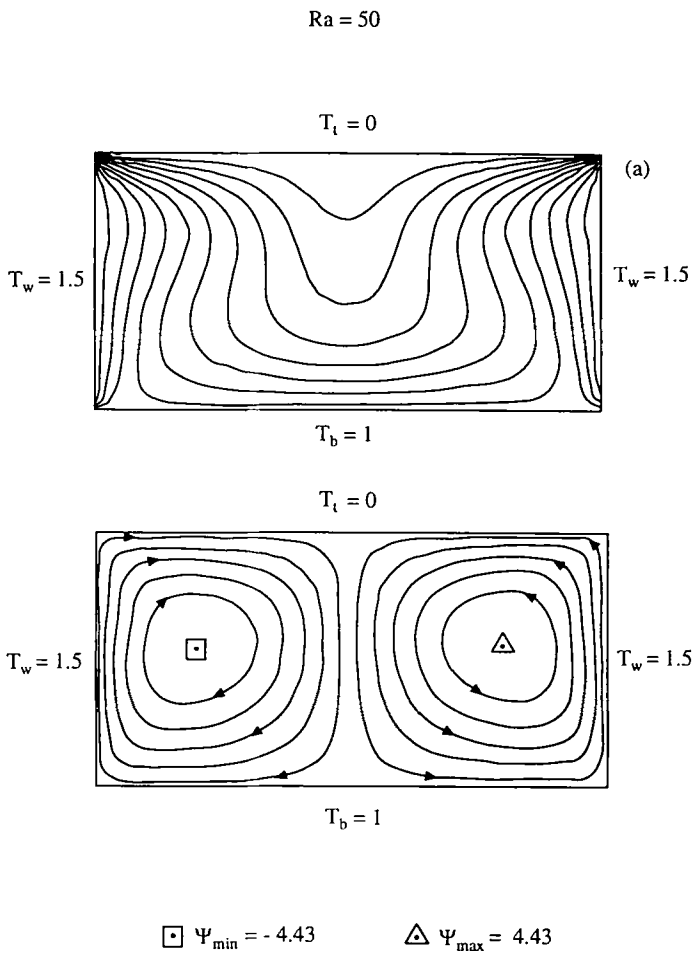

FIG. 4. Graphical representation of the numerical solutions for the flow and temperature fields for heating from below, corresponding to $Ra = 50$ and $T_w = 1.5$. (a) Ten isotherms equally divided between T_{min} and T_{max} ($T_{min} = 0$, $T_{max} = 1.5$). (b) Ten streamlines equally divided between ψ_{min} and ψ_{max} ($\psi_{min} = -4.43$, $\psi_{max} = 4.43$).

The solution for the same Rayleigh number ($Ra = 50$), but for a different value of the lateral boundary temperature, $T_w = 1.5$, corresponding to subcase (ii) and to (26b) is presented in Fig. 4. Two convection cells were also obtained for this case ($T_w = 1.5$). However, the left cell rotates in a clockwise direction. This represents an opposite direction of rotation when related to the first case ($T_w = -0.5$, Fig. 3). This change in flow direction is related to the side walls heat flux and is in complete agreement with the analytical predictions corresponding to the weak heat flux at the side walls. The flow field and temperature solutions for $T_w = 0.5$ and $Ra = 200$ are presented in Fig. 5, from which it is observed that the second vertical mode of convection is obtained. This second vertical mode, which consists of two rows of convection cells, is also a characteristic result which depends on the value of temperature imposed on the lateral boundaries. In this case $T_w = 0.5$; thus the heat flux at the side walls is directed outwards for the bottom part of the domain and downwards for the top part. This change of sign in the heat flux along the lateral walls is responsible for the creation of the second convection mode. A relatively large value of Ra was needed to obtain convection cells throughout the entire domain. When $Ra = 100$ and $T_w = 0.5$, the results show (see Fig. 6) that the convection is localized in the vicinity of the lateral walls. The second vertical mode was also obtained for this case. This is the reason for the higher Rayleigh number needed for convection to fill up the entire domain, since a higher critical Rayleigh number corresponds to the second vertical mode ($[Ra_c]_{n=2} = 16\pi^2$). For subcritical values of Ra, convection appears as a localized effect in the vicinity of the lateral walls. As the critical value of Ra is reached, the convection spreads into the interior region and fills the entire domain. This result suggests that disturbances related to the first vertical mode, which inherently exist when using a numerical solution, were naturally suppressed by the heat flux resulting from the side walls, therefore imposing the second vertical mode of convection. However, it

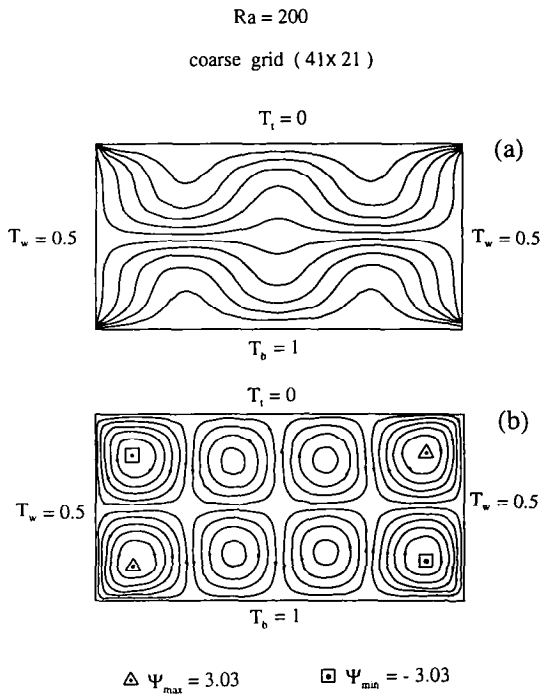

FIG. 5. Graphical representation of the numerical solutions for the flow and temperature fields for heating from below, corresponding to $Ra = 200$ and $T_w = 0.5$. (a) Ten isotherms equally divided between T_{min} and T_{max}($T_{min} = 0$, $T_{max} = 1$). (b) Ten streamlines equally divided between ψ_{min} and ψ_{max} ($\psi_{min} = -3.03$, $\psi_{max} = 3.03$).

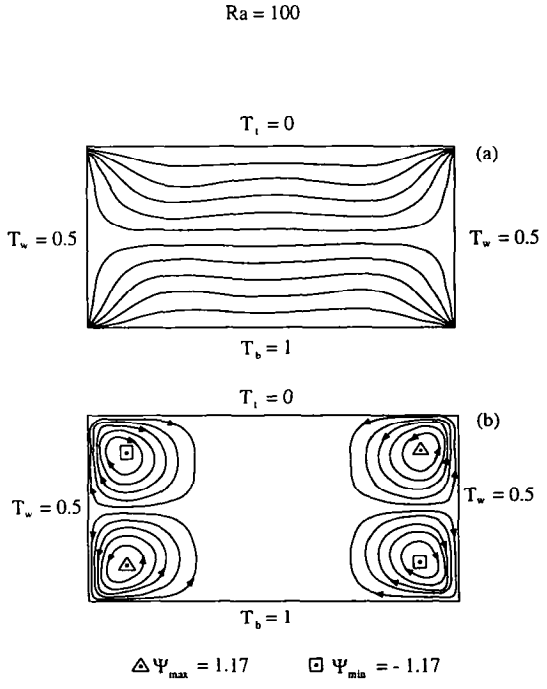

FIG. 6. Graphical representation of the numerical solutions for the flow and temperature fields for heating from below, corresponding to $Ra = 100$ and $T_w = 0.5$. (a) Ten isotherms equally divided between T_{min} and T_{max}($T_{min} = 0$, $T_{max} = 1$). (b) Ten streamlines equally divided between ψ_{min} and ψ_{max} ($\psi_{min} = -1.17$, $\psi_{max} = 1.17$).

should be mentioned that this result was obtained when using initial conditions of uniform temperature and no initial flow in the domain. Therefore it is not recommended to draw any general conclusion based on this result.

A further verification of the accuracy of the numerical results was performed for this case by using a finer grid ($\Delta L = 0.025$, 81×41) with the same parameters ($Ra = 200$, $T_w = 0.5$). A comparison of the results obtained by using the coarse (41×21) and the finer (81×41) grids showed that the maximum relative differences in the values of the stream function and temperature were less than 2%.

5.2. *Heating from above*

No convection is expected when heating from above, if the lateral boundaries are insulated. However, with perfectly conducting lateral boundaries pertaining to the present investigation, natural convection occurs as proved in Section 3. The numerical steady state solution for this case, with $Ra = 100$ and $T_w = 1.5$, is presented in Fig. 7. Two convection cells were obtained, one adjacent to the left wall and the other to the right wall. By changing the value of the side wall temperature to $T_w = -0.5$, it was observed that the flow direction is reversed. An evaluation of the accuracy of the numerical results was performed for this case by using a finer grid ($\Delta L = 0.025$, 81×41) with the same parameters ($Ra = 100$, $T_w = -0.5$). The maximum relative differences in the values of the stream function and temperature between the coarse and the finer grids were less than 6%. For $T_w = 0.5$ and $Ra = 200$, the second vertical mode is obtained (see Fig. 8), while as expected the flow direction of the convective cells was reversed when compared to the corresponding case (26c) for heating from below (Fig. 5). However, no more than two consecutive cells in the horizontal direction could be obtained. They are located adjacent to the lateral walls. This is the main difference between heating from below and heating from above. For the former (heating from below), multiple cells in the horizontal direction were created for supercritical values of the Rayleigh number and two horizontally consecutive cells of limited lateral extent adjacent to the side walls characterize the subcritical conditions. However, for the latter case (heating from above), only two horizontally consecutive cells adjacent to the side walls were obtained with possible double cells in the vertical direction depending on the value of T_w. These cells filled the entire porous domain. A finer grid ($\Delta L = 0.025$, 81×41) was also used in this case in order to evaluate the accuracy of the results leading to a maximum relative difference of 2% in the values of the stream function and temperature. The comparison of the numerical results corresponding to a strong heat flux through perfectly conducting side walls to the analytical solution obtained for a weak heat leakage through imperfectly insulated side walls shows qualitative consistency. As far as the flow direc-

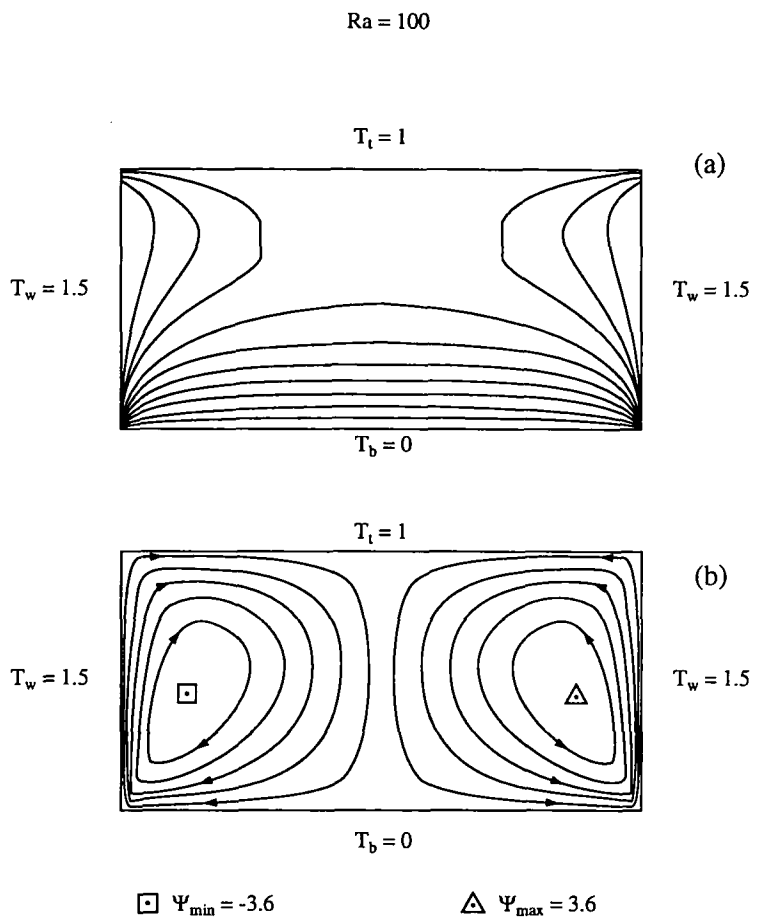

FIG. 7. Graphical representation of the numerical solutions for the flow and temperature fields for heating from above, corresponding to $Ra = 100$ and $T_w = 1.5$. (a) Ten isotherms equally divided between T_{min} and T_{max} ($T_{min} = 0$, $T_{max} = 1.5$). (b) Ten streamlines equally divided between ψ_{min} and ψ_{max} ($\psi_{min} = -3.6$, $\psi_{max} = 3.6$).

tion and the resulting wave number are concerned, the results are identical. Moreover, the side walls heat flux or temperature value was found to have a strong control over the flow intensity, direction and wave number. Therefore, carefully extending the validity of the analytical solution that is restricted to weak heat fluxes to the perfectly conducting side walls case provides a tool for a qualitative analysis even beyond the validity domain of the solution.

The conclusions from the numerical study of Kimura and Bejan [12], that the convection resulting from the imposed side wall temperature difference cannot be stabilized by imposing a stabilizing temperature gradient through heating from above, was confirmed by our results and even extended to the extreme case where no side wall temperature difference is imposed. Even then convection persists as a result of horizontal temperature gradients that are created in the fluid domain. Since results similar to Kimura and Bejan's [12] were achieved experimentally by Ostrach and Raghavan [13] for a fluid in a non-porous domain, it remains for future research to show whether our conclusions can be qualitatively extended to fluids in non-porous domains as well.

6. CONCLUSIONS

A study of natural convection in a porous medium domain heated from below or above and bounded by perfectly conducting side walls was presented. A comparison was performed between the perfectly conducting side walls case associated with strong heat fluxes through the side walls and analytical results pertaining to the imperfectly insulated side walls case (weak heat fluxes through the side walls). The comparison shows good qualitative agreement between the analytical and the numerical results. It was shown that for perfectly conducting side walls, except for a particular temperature variation on these side walls, natural convection occurs regardless of the value of the Rayleigh number and regardless of whether the fluid is heated from below or from above. The numerical solutions for identical uniform temperatures imposed on both side walls showed that when the

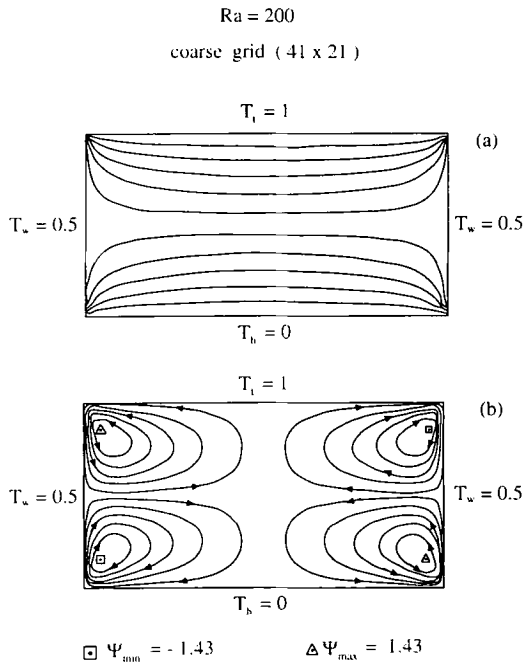

FIG. 8. Graphical representation of the numerical solutions for the flow and temperature fields for heating from above, corresponding to $Ra = 200$ and $T_w = 0.5$. (a) Ten isotherms equally divided between T_{min} and T_{max} ($T_{min} = 0$, $T_{max} = 1$). (b) Ten streamlines equally divided between ψ_{min} and ψ_{max} ($\psi_{min} = -1.43$, $\psi_{max} = 1.43$).

fluid is heated from below, a subcritical flow develops mainly in the vicinity of the side walls. Under supercritical conditions, the motion amplifies and extends over the entire porous domain. The solution was found to depend on the value of the temperature imposed on the side walls. This dependence was explained in terms of the side wall heat flux direction by extending the validity of the analytical results obtained for imperfectly insulated side walls to the present case. When the fluid was heated from above it was not possible to obtain a motionless solution, a result which is consistent with the analytical conclusions.

Acknowledgement—The authors would like to thank the Fund for the Promotion of Research at the Technion, for supporting this research.

REFERENCES

1. P. Cheng, Heat transfer in geothermal systems. In *Advances in Heat Transfer* (Edited by T. F. Irvine, Jr and J. P. Hartnett), Vol. 14, pp. 1–105. Academic Press, New York (1978).
2. P. Cheng, Geothermal heat transfer. In *Handbook of Heat Transfer Applications* (Edited by Rohsenow *et al.*), Chap. 11. McGraw-Hill, New York (1981).
3. A. Bejan and C. L. Tien, Natural convection in a horizontal porous medium subjected to an end-to-end temperature difference, *ASME J. Heat Transfer* **100**, 191–198 (1978).
4. C. W. Horton and F. T. Rogers, Convection currents in porous media, *J. Appl. Phys.* **16**, 367–370 (1945).
5. E. R. Lapwood, Convection of a fluid in a porous medium, *Proc. Cambridge Phil. Soc.* **44**, 508–521 (1948).
6. R. A. Wooding, Steady free thermal convection of a liquid in a saturated permeable medium, *J. Fluid Mech.* **2**, 273–285 (1957).
7. R. A. Wooding, An experiment on free thermal convection of water in saturated permeable material, *J. Fluid Mech.* **3**, 582–600 (1958).
8. D. A. Nield, Onset of thermohaline convection in a porous medium, *Water Resources Res.* **4**, 553–560 (1967).
9. J. W. Elder, Steady free convection in a porous medium heated from below, *J. Fluid Mech.* **27**, 29–48 (1967).
10. P. Vadasz and C. Braester, The effect of imperfectly insulated sidewalls on natural convection in porous media, *Acta Mech.* **91**, 215–233 (1992).
11. P. Vadasz, Bifurcation phenomena in natural convection in porous media, *Proc. Ninth Int. Heat Transfer Conf.* Vol. 5, pp. 147–153. (1990).
12. S. Kimura and A. Bejan, Natural convection in a stably heated corner filled with porous medium, *ASME J. Heat Transfer* **107**, 293–298 (1985).
13. S. Ostrach and C. Raghavan, Effect of stabilizing thermal gradients on natural convection in rectangular enclosures, *ASME J. Heat Transfer* **101**, 238–243 (1979).
14. M. A. Combarnous and S. A. Bories, Hydrothermal convection in saturated porous media. In *Advances in Hydrosciences* (Edited by V. T. Chow), Vol. 10, pp. 231–307. Academic Press, New York (1975).
15. G. Dagan, Some aspects of heat and mass transfer in porous media. In *Fundamentals of Transport Phenomena in Porous Media* (Edited by J. Bear), pp. 55–64. Int. Association for Hydraulic Research, Elsevier, New York (1972).
16. A. Oberbeck, Ueber die Wärmeleitung der Flüssigkeiten bei Berücksichtigung der Strömungen infolge von Temperatur-differenzen, *Ann. Phys. Chem.* **7**, 271–292 (1879).
17. J. Boussinesq, *Theorie Analitique de la Chaleur*, Vol. 2, pp. 154–176. Gauthier-Villars, Paris (1903).
18. D. H. Thurnau, Bandsolve, *Communications of ACM*, Algorithm 195, Vol. 6, No. 8, p. 441 (1963).